Supplemental Information for

Structural Insights into the Mechanism of Carbapenemase Activity of the OXA-48 β-Lactamase

Clyde A. Smith[a,#], Nichole K. Stewart[b], Marta Toth[b], Sergei B. Vakulenko[b,#]

[a] Stanford Synchrotron Radiation Lightsource, Stanford University, Menlo Park, California, USA

[b] Department of Chemistry and Biochemistry, University of Notre Dame, Notre Dame, Indiana, USA

Table S1. Some characteristics of the reported OXA-48 structures

PDB code	Crystal form	Asymmetric unit contents	Space group	Unit cell (a,b,c), Å	Resolution	*rmsd* (Å) monomer	*rmsd* (Å) dimer	ref.
this work	apo	1 dimer	$P2_12_12_1$	70.746, 76.827, 100.044[a]	1.6 Å	-	-	-
3HBR	apo	2 dimers	$P2_1$	63.701, 107.185, 80.787, β=111.04°	1.9 Å	0.32	0.37	(1)
4S2J	pH 6.5	2 dimers	$P2_12_12_1$	64.05, 108.10, 162.81	2.54 Å	0.23	0.27	(2)
4S2K	pH 7.5	2 dimers	$P3_2$	142.78, 52.42	2.1 Å	0.33	0.36	(2)
4S2P	apo	1 dimer	$P2_12_12_1$	43.41, 102.87, 124.73	1.7 Å	0.43	0.54	(2)
4WMC	avibactam	4 dimers	$P2_1$	63.886, 165.465, 108.524, β=90.39°	2.3 Å	0.32	0.35	(3)
5DVA	inhibitor	4 monomers[b]	$P2_12_12_1$	91.037, 109.66, 124.241	2.5 Å	0.26	0.31	(4)
5FAQ	inhibitor	1 dimer	$P2_12_12_1$	72.76, 75.47, 106.97[a]	1.96 Å	0.23	0.26	(5)
5HAP	S70A	1 dimer	$P6_522$	121.9, 161.451	1.89 Å	0.31	0.59	(6)
5HAQ	S70G	1 dimer	$P2_12_12_1$	72.66, 73.611, 106.36[a]	2.14 Å	0.21	0.30	(6)
5OFT	R206A	1 dimer	$P6_522$	120.151, 160.107	3.2 Å	0.36	0.65	(7)
5QB4	imipenem	4 monomers[b]	$P2_12_12_1$	88.79, 107.5, 124.33	1.95 Å	0.33	0.35	(8)
6GOA	R189A	4 dimers	$P2_1$	107.726, 85.545, 125.805, β=90.08°	2.55 Å	0.27	0.39	(7)

[a] Crystallization buffer contains divalent cation(s)

[b] The dimer is formed by crystallographic symmetry

Table S2. OXA-48 crystallization conditions

Screen[a]	Composition	Space group	Unit cell (a,b,c), Å	Resolution
-	0.1 M HEPES pH 7.5, 8% 1-butanol, 10% PEG 8000	$P2_1$	63.7, 107.2, 80.8, β=111º	2.5 Å
PEG/Ion1 #31	0.2 M $LiSO_4$, 20% PEG3350	C222	80.4, 107.8, 125.5	1.8 Å
PEG/Ion2 #5	0.1 M Na malonate pH 6, 12% PEG3350	$P2_1$	89.7, 108.0, 125.7, β=109.5°	2.1 Å
PEG/Ion2 #6	0.2 M Na malonate pH 6, 20% PEG3350	P222	81.0, 108.0, 125.7	2.3 Å
PEG/Ion2 #8	0.2 M Na malonate pH 7, 20% PEG3350	P222	81.4, 107.6, 125.6	2.0 Å
PEG/Ion2 #13	4% tacsimate pH 6, 12% PEG3350	P222	94.8, 108.5, 125.5	2.5 Å
PEG/Ion2 #23	0.1 M DL-malic acid pH 7, 12% PEG3350	$P2_1$	92.4, 108.5, 124.3, β=96.6°	1.9 Å
PEG/Ion2 #37	0.06 M citrate/0.06M BTP pH 4.1, 16% PEG3350	$P2_1$	83.8, 106.2, 126.3, β=109.3°	2.4 Å
PEG/Ion2 #42	20 mM $CaCl_2$, 20 mM $CdCl_2$, 20 mM $CoCl_2$, 20% PEG3350	$P2_12_12_1$	70.8, 76.8, 100.1	1.6 Å

[a] Hampton screen number (www.hamptonresearch.com)

TABLE S3. OXA-48 data collection statistics[a]

	Apo	Imipenem	Meropenem	Ertapenem	Doripenem
Beamline	BL12-2	BL12-2	BL12-2	BL9-2	BL12-2
Unit cell, a, b, c (Å)	70.75, 76.83, 100.04	72.13, 76.21, 101.13	73.13, 74.56, 97.97	71.88, 76.82, 101.25	72.60, 76.75, 101.19
Resolution (Å)	38.4-1.4 (1.43-1.4)	38.1-1.8 (1.84-1.8)	36.6-1.75 (1.78-1.75)	38.4-2.25 (3.32-2.25)	38.4-1.9 (1.94-1.9)
Reflections					
- observed/unique	953017 / 72537	384411 / 52357	537328 / 53334	196639 / 27260	329979 / 44627
R_{meas}[b]	10.5 (259.1)	10.0 (132.4)	9.8 (140.0)	14.2 (183.6)	14.2 (215.7)
R_{pim}[c]	2.9 (71.8)	3.6 (48.6)	3.1 (44.5)	5.2 (67.9)	5.2 (82.9)
I / σI	13.8 (1.7)	10.9 (1.9)	13.3 (1.9)	8.5 (1.4)	10.4 (2.4)
Completeness (%)	99.9 (99.2)	99.8 (97.3)	97.8 (97.0)	99.9 (99.3)	98.7 (97.0)
CC½[d]	0.999 (0.581)	0.998 (0.668)	0.996 (0.781)	0.997 (0.723)	0.995 (0.538)
Average multiplicity	13.1 (12.7)	7.3 (7.2)	10.1 (9.6)	7.2 (7.3)	7.4 (7.2)
Wilson B (Å^2)	23.9	26.9	23.6	45.6	29.0

[a] Numbers in parentheses refer to the highest resolution shell
[b] R_{meas} is the redundancy-independent merging R factor (9)
[c] R_{pim} is the precision-indicating merging R factor (9)
[d] Correlation between intensities from random half-sets of data (10)

TABLE S4. OXA-48 structure refinement statistics

	Apo	Imipenem	Meropenem	Ertapenem	Doripenem
PDB Code	6P96	6P97	6P98	6P99	6P9C
Resolution (Å)	38.4-1.4	38.1-1.8	36.6-1.75	38.4 – 2.25	39.1-1.9
Reflections, work/free	72372 / 3574	52223 / 2698	53295 / 2749	27178 / 1403	44388 / 2254
R_{work} / R_{free}[a]	0.1838 / 0.2089	0.1721 / 0.2026	0.1886 / 0.2204	0.1984 / 0.2568	0.1942 / 0.2410
Number of atoms					
- protein	1992 (A), 2006 (B)	1988 (A), 2000 (B)	2015 (A), 1979 (B)	1974 (A), 1985 (B)	2013 (A), 1983 (B)
- water	362	365	283	70	182
- ligands	-	40	52	33	54
B-factors (Å^2)					
- protein	25.0 (A), 26.9 (B)	25.8 (A), 31.8 (B)	23.2 (A), 28.2 (B)	42.8 (A), 50.1 (B)	28.9 (A), 33.6 (B)
- water	34.1	34.6	30.8	44.0	32.8
- ligands	-	44.5 (A), 52.8 (B)	32.1 (A), 37.6 (B)	58.7[b]	42.0 (A), 51.8 (B)
rms deviations					
- bond lengths (Å)	0.006	0.007	0.007	0.008	0.007
- bond angles (°)	0.79	0.95	1.02	1.02	1.55
Ligand occupancies (%)					
- core	-	100 (A), 100 (B)	100 (A), 100 (B)	100 (A)	100 (A), 100 (B)
- tail	-	75 (A), 83 (B)	78 (A), 77 (B)	89 (A)	80 (A), 57 (B)
RSCC values for ligand[c]	-	0.82 (A), 0.80 (B)	0.89 (A), 0.79 (B)	0.81 (A)	0.86 (A), 0.67 (B)
Ramachandran plot[d]					
- favored region (%)	97.1	97.5	97.7	95.4	96.9
- outliers	2	0	0	1	3
Molprobity Score[d]	1.11	1.18	1.15	1.40	1.39

[a] R_{free} was calculated using a test set comprising 5% of the data
[b] Ertapenem was built into monomer A only
[c] From PDB validation
[d] Calculated with the program MOLPROBITY (11)

Supplementary Figures

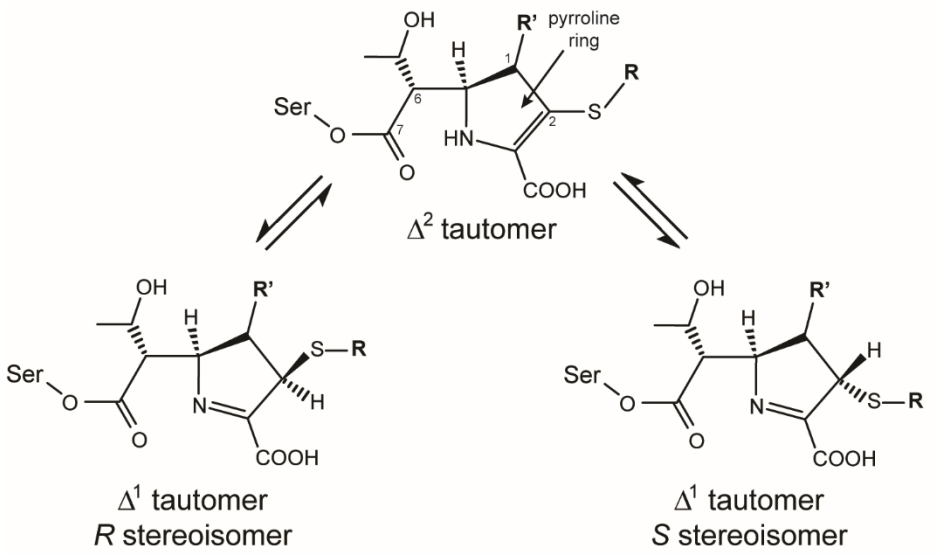

Supplementary FIG S1. Tautomerization of the pyrroline ring of acylated carbapenems. The **R** group attached to the exocyclic sulfur represents the tail group of the various carbapenems (see Fig. 1). The **R'** group at the C1 carbon is either hydrogen in imipenem or a methyl group in meropenem, ertapenem and doripenem.

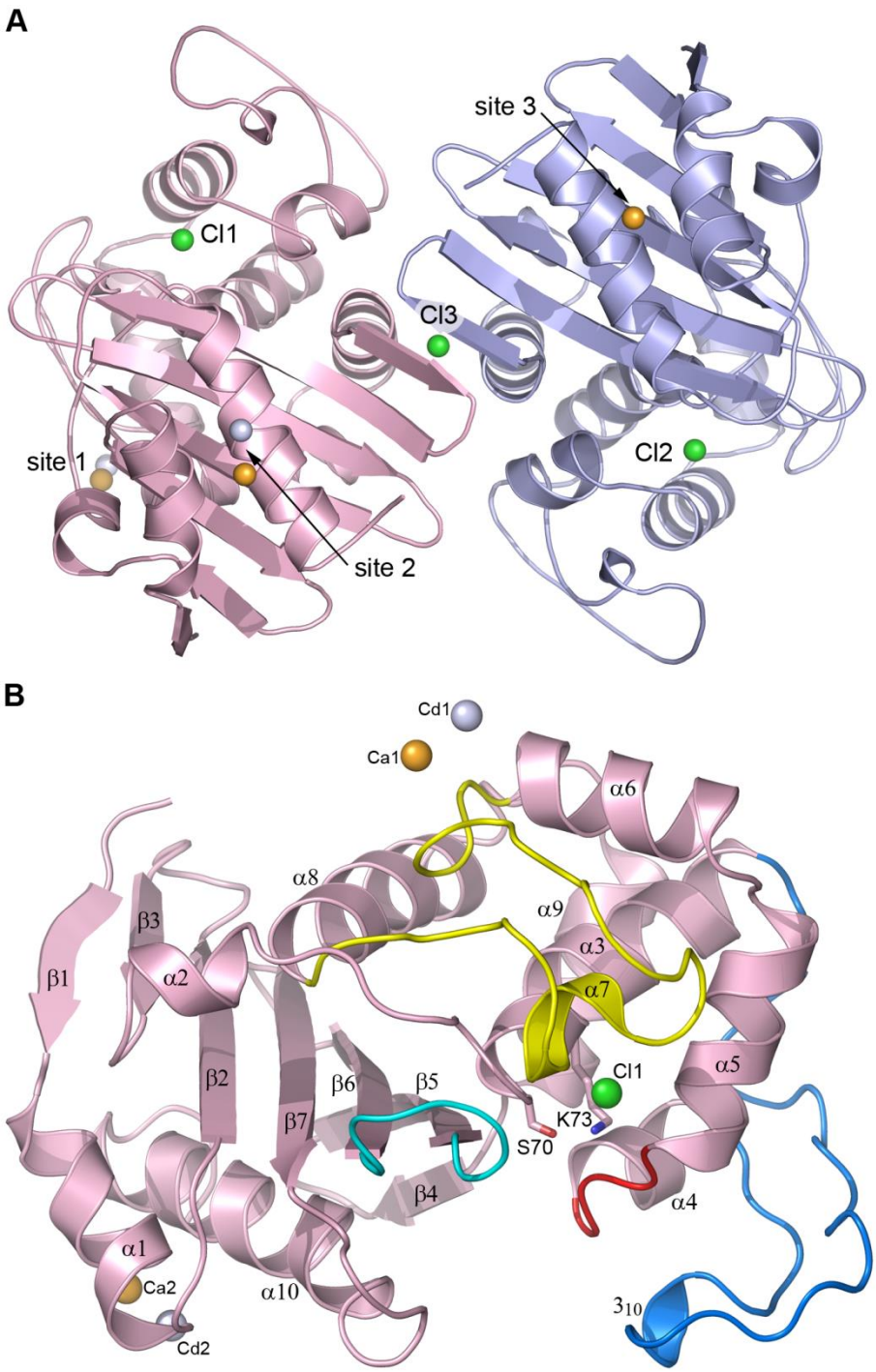

Supplementary FIG S2. (A) Ribbon representation of the apo-OXA-48 dimer (monomer A pink and monomer B blue), oriented such that the non-crystallographic symmetry (NCS) two-fold axis is pointing into the page. The two chloride ions in the active site of each monomer (Cl1 and Cl2) are indicated as green spheres. The third chloride ion (Cl3), which bridges between the

two monomers, is located on the NCS two-fold axis. The location of the three metal sites are shown (calcium colored orange, cadmium colored gray). (B) The apo-OXA-48 monomer A structure (pink ribbons) showing the secondary structure labeling. The four metal ions associated with this monomer are indicated. Four loops highlighted in the text are colored yellow (the Ω-loop), red (the α4-α5 loop), cyan (the β5-β6 loop) and blue (the long α3-α4 loop). The location of the active site is given by the side chains of Ser70 and Lys73, and by the chloride ion Cl1.

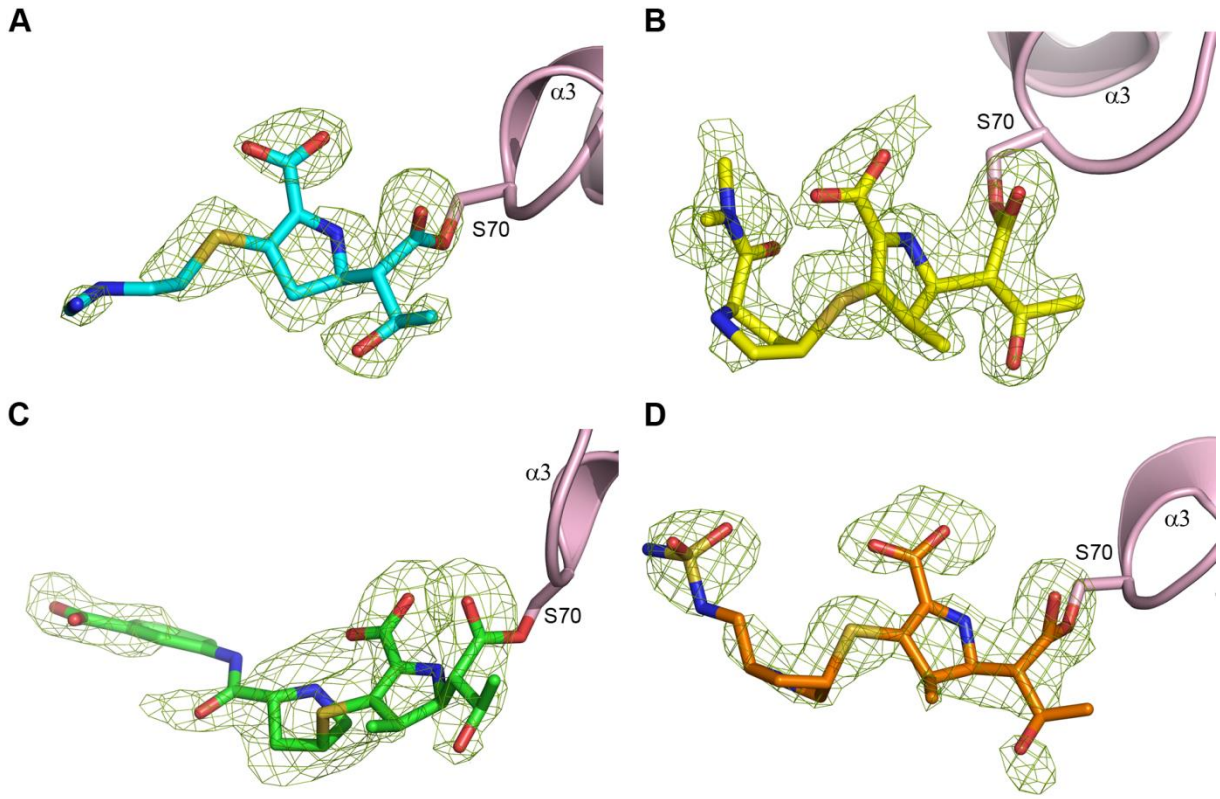

Supplementary FIG S3. Polder OMIT maps (green mesh) for (A) imipenem, (B) meropenem, (C) ertapenem and (D) doripenem. All maps were calculated at the end of refinement using PHENIX.POLDER (12), and contoured at 2.5 σ. The final refined models of each carbapenem is shown superimposed upon the OMIT maps.

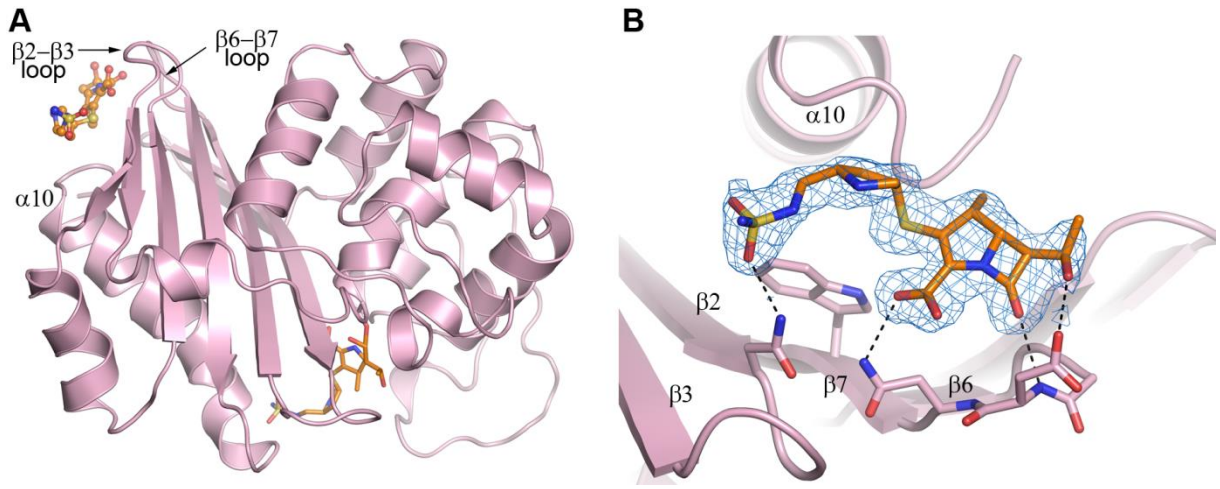

Supplementary FIG S4. The non-hydrolyzed doripenem. (A) Ribbon representation of the doripenem-OXA-48 complex showing the location of the non-hydrolyzed doripenem molecule as a ball-and-stick model at the upper left. The acylated doripenem in the active site is also shown as sticks (lower center). (B) Final refined $2F_o$-F_c electron density for the non-hydrolyzed doripenem, showing the interactions it makes with residues from the β2-β3 and β6-β7 loops.

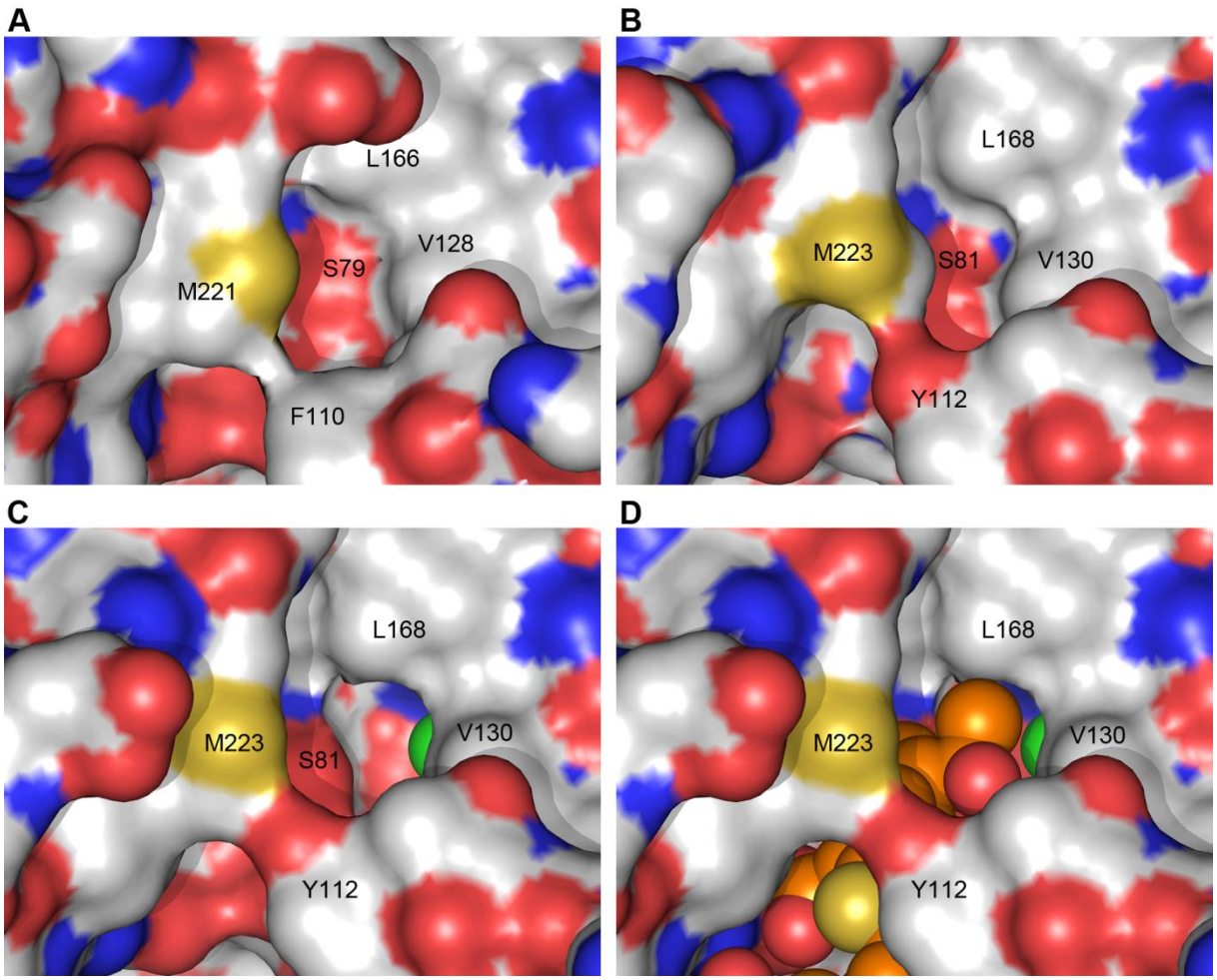

Supplementary FIG S5. Molecular surfaces of OXA-23 and OXA-24/40. (A) The surface of apo-OXA-23 showing the closed surface between the hydrophobic patch (Leu166 and Val128) and the catalytic serine (Ser79). (B) The surface of apo-OXA-24/40 showing the closed surface between the hydrophobic patch (Leu168 and Val130) and the catalytic serine (Ser81). (C) The surface calculated for the doripenem-OXA-24/40 complex with doripenem removed, showing the channel that opens upon rotation of the Val130 side chain. The green sphere marks where the carboxylated lysine would be in the deacylation water pocket in an activated enzyme. (D) The same surface as in panel (C) with doripenem shown as orange CPK spheres, with the channel still partially open and accessible. In all cases the hydrophobic bridge across the active site (M221-F110 in OXA-23, and M223-Y112 in OXA-24/40) is evident.

Supplementary References

1. Docquier JD, Calderone V, De Luca F, Benvenuti M, Giuliani F, Bellucci L, Tafi A, Nordmann P, Botta M, Rossolini GM, Mangani S. 2009. Crystal structure of the OXA-48 β-lactamase reveals mechanistic diversity among class D carbapenemases. Chem Biol 16:540-547.
2. King DT, King AM, Lal SM, Wright GD, Strynadka NC. 2015. Molecular mechanism of avibactam-mediated β-lactamase inhibition. ACS Infect Dis 1:175-184.
3. Lahiri SD, Mangani S, Jahic H, Benvenuti M, Durand-Reville TF, De Luca F, Ehmann DE, Rossolini GM, Alm RA, Docquier JD. 2015. Molecular basis of selective inhibition and slow reversibility of avibactam against class D carbapenemases: A structure-guided study of OXA-24 and OXA-48. ACS Chem Biol 10:591-600.
4. Lund BA, Christopeit T, Guttormsen Y, Bayer A, Leiros HK. 2016. Screening and design of inhibitor scaffolds for the antibiotic resistance oxacillinase-48 (OXA-48) through surface plasmon resonance screening. J Med Chem 59:5542–5554.
5. King AM, King DT, French S, Brouillette E, Asli A, Alexander JA, Vuckovic M, Maiti SN, Parr TR, Brown ED, Malouin F, Strynadka NC, Wright GD. 2016. Structural and kinetic characterization of diazabicyclooctanes as dual inhibitors of both serine-β-lactamases and penicillin-binding proteins. ACS Chem Biol 11:864-868.
6. Stojanoski V, Adamski CJ, Hu L, Mehta SC, Sankaran B, Zwart P, Prasad BV, Palzkill T. 2016. Removal of the side chain at the active-site serine by a glycine substitution increases the stability of a wide range of serine β-lactamases by relieving steric strain. Biochemistry 55:2479-2490.

7. Lund BA, Thomassen AM, Nesheim BHB, Carlsen TJO, Isaksson J, Christopeit T, Leiros HS. 2018. The biological assembly of OXA-48 reveals a dimer interface with high charge complementarity and very high affinity. FEBS J 285:4214-4228.

8. Akhter S, Lund BA, Ismael A, Langer M, Isaksson J, Christopeit T, Leiros HS, Bayer A. 2018. A focused fragment library targeting the antibiotic resistance enzyme Oxacillinase-48: Synthesis, structural evaluation and inhibitor design. Eur J Med Chem 145:634-648.

9. Weiss MS. 2001. Glocal indicators of X-ray data quality. J Appl Crystallogr 34:130-135.

10. Karplus PA, Diederichs K. 2012. Linking crystallographic model and data quality. Science 336:1030-1033.

11. Chen VB, Arendall WB, Headd JJ, Keedy DA, Immormino RM, Kapral GJ, Murray LW, Richardson JS, Richardson DC. 2010. MolProbity: All-atom structure validation for macromolecular crystallography. Acta Crystallogr D66:12-21.

12. Liebschner D, Afonine PV, Moriarty NW, Poon BK, Sobolev OV, Terwilliger TC, Adams PD. 2017. Polder maps: Improving OMIT maps by excluding bulk-solvent. Acta Crystallogr D73:148-157.